Chaos in Practically Isolated Microcavity Lasers

Sebastian Wieczorek and Weng W. Chow
Semiconductor Material and Device Sciences Department, Sandia National Laboratories, Albuquerque, New Mexico 87185-0601, USA
(Received 2 October 2003; published 27 May 2004)

We report that essentially isolated microcavity lasers may interact in the most complicated manner and drive each other chaotic. As the optical isolation between these lasers reaches presently practically attainable limits, instead of approaching independent operation, the lasers exhibit mutually induced chaotic oscillations. The chaos arises from an intricate coupling of the nonlinearities associated with coupled optical resonators and those evolving from the population dynamics in the active region. The investigation is performed using a composite-cavity theory and a class-*B* description of the gain medium. Bifurcation analysis identifies the source of instabilities and determines their robustness.

DOI: 10.1103/PhysRevLett.92.213901 PACS numbers: 42.65.Sf, 02.30.Oz, 05.45.Xt, 42.55.Sa

Interacting nonlinear oscillators are intensively studied for their rich dynamics, including a variety of bifurcations (instabilities), chaotic oscillations, and ability to synchronize at different modes of operation [1,2]. Lasers play an important role in these pursuits [3,4]. Coupled lasers constitute experimentally realizable examples of interacting nonlinear oscillators [3] and are used in many device applications. Hence, the physics of interacting lasers is of fundamental interest, on the one hand, and of great technological importance, on the other hand.

Most of the recent studies focusing on coupled lasers deal with effects of delay in the coupling [5], global coupling via mean field [6], and different types of synchronization [7–10]. Less attention is devoted to dynamical properties of practically uncoupled lasers, although such lasers are encountered in a wide range of applications. By practically uncoupled or isolated lasers, we mean two or more lasers where the desire is for the lasers to operate totally independent of one another, while in practice, only partial isolation is possible. Practically isolated lasers are encountered in the modern technology of micro-optical circuits, where one faces the problem of reducing cross talk between laser diodes integrated onto a single chip. In laser gyros, the lockband that is detrimental to device performance is directly related to the minute amount of backscattering coupling the counterpropagating modes.

Totally isolated lasers lase independently and at frequencies determined solely by the resonances of the separate optical resonators. Consequently, the beatnote between two lasers $\dot{\psi}_{AB}$ is a linear function of the difference between resonator optical path lengths dL, as depicted in Fig. 1(a). On the other hand, in the presence of coupling, the beat note has two extrema and exhibits a lockband, as may be seen in Fig. 1(b). It is generally believed that the transition from Fig. 1(a) to Fig. 1(b) occurs smoothly, i.e., with an uninterrupted vanishing of the lockband as the coupling approaches zero. Instead, we discovered that the approach from coupled to completely isolated laser behavior can be accompanied by the occurrence of mutually induced instabilities and chaos.

Our result is obtained through an investigation of coupled-laser behavior under the conditions of very weak coupling and nearly identical lasers. The analysis starts with expanding the laser field in terms of passive-cavity eigenmodes $u_n(z)$:

$$\mathcal{E}(z,t) = \frac{1}{2}\sum_n [E_n(t)e^{-i\psi_n(t)}u_n(z) + \text{c.c.}]. \qquad (1)$$

We assume plane wave conditions, z is along the field propagation direction, t is time, and E_n and ψ_n are the time-dependent electric field amplitude and phase. There are two approaches to treating the passive-cavity modes. In what is customarily referred to as an individual-cavity theory, the coupling is ignored in $u_n(z)$, which is the eigenfunction of an individual cavity. Rather, it appears in the laser field amplitude and phase equations of motion. Each equation consists of a free-running laser part, plus the contributions from the other lasers in the form of an *ad hoc* driving force, whose magnitude is determined phenomenologically [7,10,11]. The second approach, which is chosen for our study, is based on including coupling effects in the passive-cavity modes. This is accomplished by treating the coupled lasers as a single

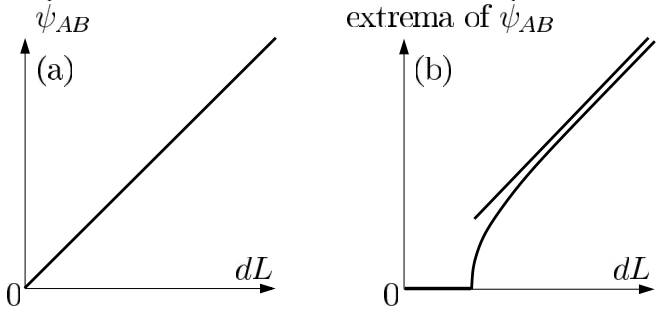

FIG. 1. (a) Laser frequency difference $\dot{\psi}_{AB}$ for totally isolated lasers and (b) extrema of $\dot{\psi}_{AB}$ for coupled lasers, versus the cavity length difference dL.

system, so that the passive-cavity modes (composite-cavity modes) $u_n(z)$ are those for the *entire* multilaser structure, including coupling [12]. This approach has two benefits that are crucial to our investigation. One is that it provides a consistent (rather than phenomenological) relationship between the system eigenfunctions and eigenfrequencies, and the effective light transmission from one laser to the other. Second, in contrast to the individual-cavity theory, modal nonlinearities due to the coupling are taken into account. These nonlinearities, when coupled to the active medium dynamics, give rise to the complex bifurcation structures that we observe in practically isolated lasers.

To illustrate the general physical phenomenon, we consider two end-to-end positioned lasers separated by a highly reflecting mirror of transmission T, as sketched in Fig. 2. The imperfect isolation is modeled as a dielectric "bump" in the background dielectric function [13] $\epsilon_b(z) = n_b^2 + \eta\delta(z)/k$, where $\delta(z)$ is the Dirac delta function, k is the wave vector in vacuum, n_b is the background refractive index, and the coefficient η is given by $2n_b\sqrt{(1-T)/T}$. Details on the composite-cavity eigenmodes and modal nonlinearities for a two-coupled-laser geometry may be found in Ref. [14]. Examples of the two composite-cavity eigenmodes with the boundary conditions $u(-L) = u(L + dL) = 0$ are illustrated in Fig. 2.

From Eq. (1) and semiclassical laser theory, one obtains the equations of motion for the amplitudes and phases of the in-phase ($n = i$) and out-of-phase ($n = o$) composite-cavity modes [15]

$$\dot{E}_n = -\frac{\Gamma_E}{2}E_n + C_{nn}\sum_{k=i,o}\left\{\frac{c}{n_b}[C_{kn}^A g^A + C_{kn}^B g^B]\cos(\psi_{kn}) + \frac{\nu}{n_b}[C_{kn}^A \delta n^A + C_{kn}^B \delta n^B]\sin(\psi_{kn})\right\}E_k, \tag{2}$$

$$\dot{\psi}_n = \Omega_n - C_{nn}\sum_{k=i,o}\left\{\frac{\nu}{n_b}[C_{kn}^A \delta n^A + C_{kn}^B \delta n^B]\cos(\psi_{kn}) - \frac{c}{n_b}[C_{kn}^A g^A + C_{kn}^B g^B]\sin(\psi_{kn})\right\}\frac{E_k}{E_n}, \tag{3}$$

where Γ_E is the composite-cavity decay rate, Ω_n is the passive composite-mode frequency, and $\psi_{kn} = \psi_k - \psi_n$ is the phase difference between the lasing composite modes. The modal integrals [15] are $C_{nk} = C_{nk}^A + C_{nk}^B$, where

$$C_{nk}^A = \frac{1}{L}\int_{-L}^{0} dz u_n(z)u_k(z),$$

$$C_{nk}^B = \frac{1}{L}\int_{0}^{L+dL} dz u_n(z)u_k(z),$$

depend on T and dL. We assume an active medium gain that is linear around threshold $g^{A(B)} = g_{\text{thr}} + \xi(N_{A(B)} - N_{\text{thr}})$, where ξ is the differential gain, N_{thr} is the threshold population density, and the threshold gain $g_{\text{thr}} = n_b\Gamma_E/2c$. Furthermore, we use the linewidth enhancement factor α to quantify the population induced refractive-index change: $\delta n^{A(B)} = -c\alpha\xi N_{A(B)}/\nu$. Under class-$B$ laser conditions (Ref. [3], Sec. 1.4), which apply to a wide variety of lasers including semiconductor lasers, field equations are coupled to the population density dynamics. The equation of motion of each laser population is [15]

$$\dot{N}_{A(B)} = \Lambda_{A(B)} - \Gamma_N N_{A(B)} - \frac{\epsilon_0\epsilon_b}{\hbar\nu}\sum_{m,n=i,o} C_{nm}^{A(B)}\frac{c}{n_b}g^{A(B)}\cos(\psi_{nm})E_mE_n, \tag{4}$$

where Λ_n is the pump rate and Γ_N is the population decay rate.

Equations (2)–(4) are solved with bifurcation continuation techniques [16] using $\Gamma_E = 5\times10^{11}\ \text{s}^{-1}$, $\Gamma_N = 10^9\ \text{s}^{-1}$, $\xi = 5\times10^{-20}\ \text{m}^2$, and $N_{\text{thr}} = 2.5\times10^{24}\ \text{m}^{-3}$. For both microcavity lasers, $L = 10\lambda/n_b = 2.8\ \mu\text{m}$, where $\lambda = 2\pi c/\nu = 0.952\ \mu\text{m}$ is approximately the wavelength of a free-running laser. The lasers operate at twice threshold.

Figure 3 depicts the bifurcation diagram in the $(T, dL/\lambda)$ plane, where bifurcations of attractors (called supercritical) are plotted with solid curves, and bifurcations of unstable objects (called subcritical and needed for consistent dynamical picture) are plotted with dashed curves. The lockband [Fig. 3(a)], where the lasers operate with a single composite-cavity mode, is indicated by the region between the two supercritical branches of Hopf bifurcation curve H. The locked state is lost when H is crossed towards higher values of $|dL|$. No other transition is visible at this scale, and the general features at moderate coupling are similar to those obtained with an individual-cavity theory.

However, the coupled-laser behavior contains an anomaly, whose presence is noticeable only with significant magnification of the $(T, dL/\lambda)$ parameter space in the vicinity of the origin [Fig. 3(b)]. There, we find the curves of saddle-node and Hopf bifurcations, S and H,

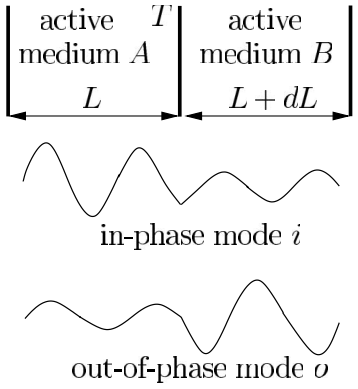

FIG. 2. (Top) Two lasers separated with a mirror of transmission T. (Bottom) Passive composite-cavity modes for $dL > 0$.

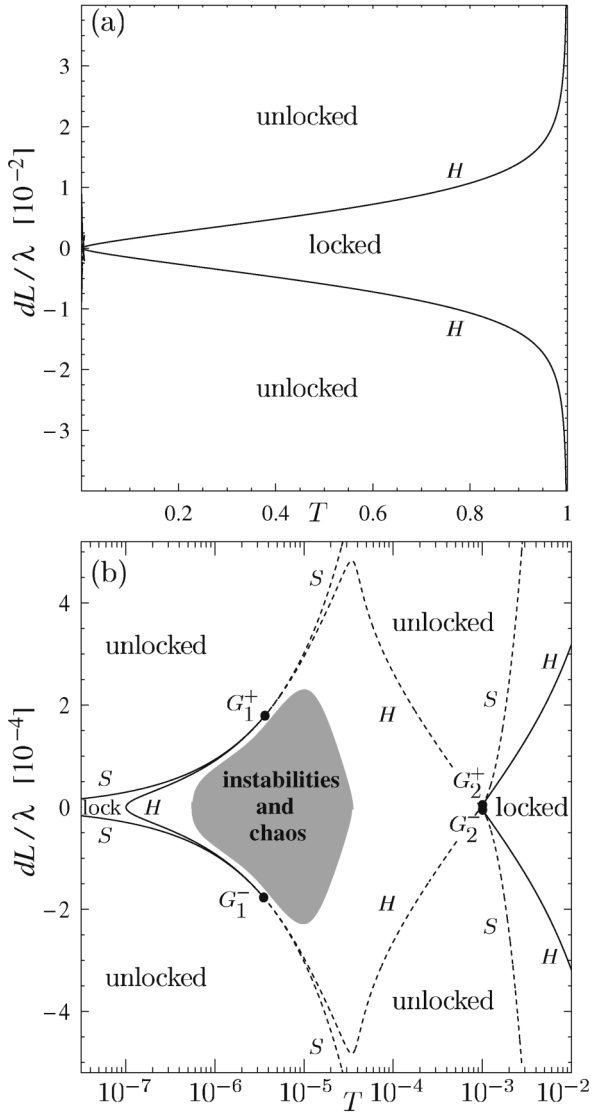

FIG. 3. (a) Bifurcation diagram for coupled microcavity lasers. (b) Expanded plot for small T and dL/λ.

respectively. These curves are tangent at four locations, and they change from subcritical to supercritical at the tangency points G. These are codimension-two saddle-node–Hopf points, or organizing centers that are often origins of complex bifurcation structures that give rise to chaos [1]. Starting from the right, the locking region closes near G_2^+ and G_2^- where the two branches of S merge. The lockband reappears at G_1^+ and G_1^- and ends at the origin of the $(T, dL/\lambda)$ plane. In the notation of Ref. [1] G_1 and G_2 belong to different types of saddle-node–Hopf points. While G_2^+ and G_2^- are essentially responsible for the termination of the locking region, G_1^+ and G_1^- are associated with a complex web of bifurcations. We found interconnected torus bifurcation, cascades of period-doubling bifurcation and saddle-node of limit cycle bifurcation curves extending between G_1^+ and G_1^-. For clarity, we shaded the region of complicated and chaotic dynamics in Fig. 3(b), instead of plotting the complex web of bifurcation curves.

Figure 4 shows an example of the complicated dynamics occurring at the ultraweak coupling. The first instability, at $dL/\lambda \approx |3 \times 10^{-4}|$, is period-doubling bifurcation. Then, there is a sequence of secondary period doublings leading to formation of a "small" chaotic attractor. At $dL/\lambda \approx |2.4 \times 10^{-4}|$ the size of the chaotic attractor suddenly and significantly increases due to interior crisis [17]. While the results shown in Fig. 4 are for $T = 5 \times 10^{-6}$, they represent the dynamics for $7 \times 10^{-7} < T < 4 \times 10^{-5}$.

The chaotic oscillations at ultraweak coupling should be experimentally observable as they manifest in distinct optical spectra. Figure 5 shows the phase portraits of the system described by Eqs. (2)–(4), and the corresponding spectra of the intracavity electric field of lasers A and B, for three situations. For $T > 10^{-3}$ and within the lock-band, both lasers operate with the out-of-phase mode represented by the fixed point in Fig. 5(a). Their spectra are identical with a peak at $\dot{\psi}_o$ (henceforth, the reference frequency). When unlocked, the lasers operate at different frequencies and exhibit slow oscillations at the beat note frequency $\dot{\psi}_{io}$ [periodic orbit, Fig. 5(b)]. For each laser, the spectrum shows side peaks detuned $\dot{\psi}_{io}$ from its main-frequency peak. Coupled-laser spectra change significantly in the chaotic region. The chaotic oscillations at ultraweak coupling are characterized by a continuum of frequencies resulting in broad and continuous spectra with little traces of periodic components [Fig. 5(c)]. Because of the sensitivity to experimental parameters, a concern is the influence of parametric noise (e.g., due to the thermal fluctuations). The time scale of such fluctuations is typically several orders of magnitude slower than that of the reported oscillations ($\approx$1 ps) and,

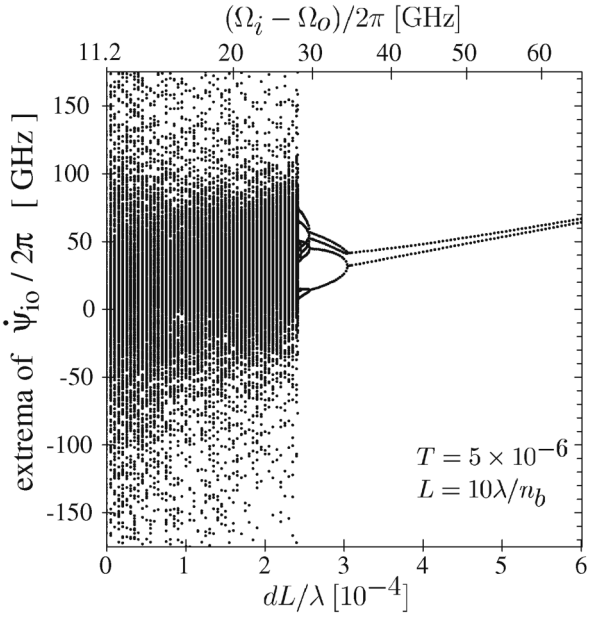

FIG. 4. Extrema of the beat note $\dot{\psi}_{io}$ versus the normalized cavity length difference dL/λ. Also given is the corresponding passive composite-mode detuning $\Omega_i - \Omega_o$.

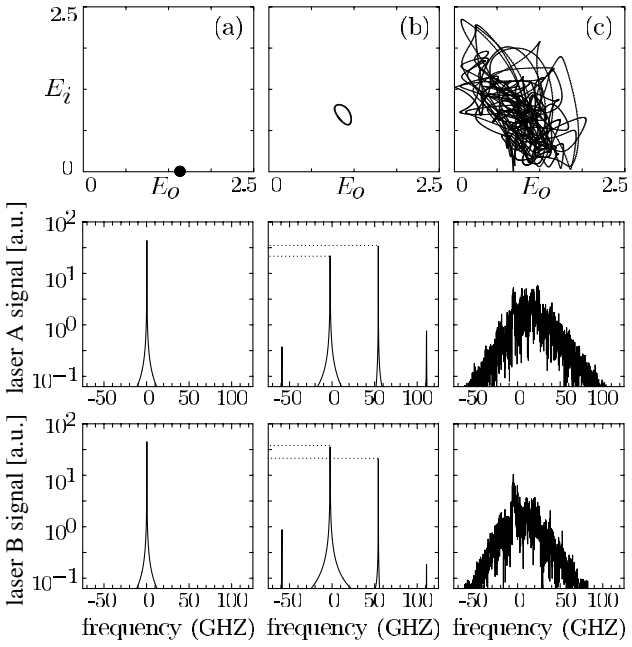

FIG. 5. (a) Locked, (b) periodic-unlocked, and (c) chaotic-unlocked dynamics shown in (upper row) phase portraits [projection onto (E_o, E_i) plane, where $E_{o(i)}$ is in units of a single-laser field] and in the corresponding optical spectra of (middle row) laser A and (bottom row) laser B. $\Delta L/\lambda = 10^{-4}$ and from (a) to (c) $T = 10^{-2}$, 10^{-4}, and 10^{-5}.

consequently, would be distinguishable experimentally. If the regions of different "fast" dynamics from Fig. 3(b) are visited due to the "slowly" fluctuating noise, the observed spectrum will be a mixture of the spectra from Fig. 5.

The positions of the organizing centers G_1^+ and G_1^- and associated bifurcation structures in the bifurcation diagram depend strongly on the coupled-laser geometry. For example, as the cavity length L increases, the instabilities migrate towards higher values of T, so that for $L \gtrsim 1$ mm, the chaotic region occurs at moderately high coupling. Chaotic behavior in coupled conventional lasers has been observed [10], and the chaos described in this Letter is its mutation in the ultraweak coupling regime. However, noticeable differences in signature exist because the effects of modal nonlinearities are significantly larger at ultraweak coupling. The bifurcation diagram shown in Fig. 3(b) depends on α. While some chaos remains even for $\alpha = 0$, the bifurcation structure can change substantially.

In summary, this Letter describes an investigation of two practically isolated microcavity lasers, i.e., imperfectly isolated microcavity lasers where some minute coupling remains. We discover interesting dynamics arising from nonlinearities imparted in the modal properties by the optical coupling, and in the complex susceptibility of the active medium by the population dynamics. Their interplay amplifies, resulting in a rich display of chaotic oscillations, when two conditions are met simultaneously. (i) The composite-mode beat note must be close to resonant with the characteristic (relaxation oscillation) frequency of the active medium, thus strongly coupling laser fields and active media. (ii) Appreciable overlap between composite-cavity modes must be present to strongly couple (via spatial hole burning) the lasing modes. For short cavities these two conditions may be satisfied at ultralow optical coupling (e.g., $T \lesssim 10^{-5}$ for $L \sim 3\lambda$), resulting in chaotic oscillations interrupting the otherwise smooth transition from coupled to totally independent operation. To accurately describe the nonlinearities and their intricate interplay, we use a composite-cavity theory for the lasing modes and a class-B description of the active medium. Additionally, bifurcation analysis is used to map the relevant parameter space, in order to identify the source of the instabilities and determine their robustness. Our study uncovers an intriguing and counterintuitive example of coupled nonlinear oscillator behavior.

We thank B. Krauskopf for stimulating discusions. This work is supported in part by the U.S. Department of Energy under Contract No. DE-AC04-94AL8500 and the Alexander von Humboldt Foundation.

[1] J. Guckenheimer and P. Holmes, *Nonlinear Oscillations, Dynamical Systems, and Bifurcations of Vector Fields* (Springer, New York, 1995).
[2] S. H. Strogatz, Physica (Amsterdam) **143D**, 1 (2000).
[3] C. O. Weiss and R. Vilaseca, *Dynamics of Lasers* (VCH Verlagsgesellschaft, Wenheim, Germany, 1991).
[4] *Fundamental Issues of Nonlinear Laser Dynamics*, edited by B. Krauskopf and D. Lenstra, AIP Conf. Proc. No. 548 (2000).
[5] G. Kozyreff, A. G. Vladimirov, and P. Mandel, Phys. Rev. Lett. **85**, 3809 (2000).
[6] R. Oliva and S. H. Strogatz, Int. J. Bifurcation Chaos Appl. Sci. Eng. **11**, 2355 (2001).
[7] H. G. Winful and L. Rahman, Phys. Rev. Lett. **65**, 1575 (1990).
[8] R. Roy and K. S. Thornburg, Jr., Phys. Rev. Lett. **72**, 2009 (1994).
[9] A. Hohl *et al.*, Phys. Rev. Lett. **78**, 4745 (1997).
[10] K. S.Thornburg, Jr. *et al.*, Phys. Rev. E **55**, 3865 (1997).
[11] A. I. Khibnik *et al.*, Physica (Amsterdam) **111D**, 295 (1998).
[12] S. A. Shakir and W.W. Chow, Opt. Lett. **9**, 202 (1984).
[13] M. B. Spencer and W. E. Lamb, Jr., Phys. Rev. A **5** , 893 (1972).
[14] W.W. Chow, IEEE J. Quantum Electron. **QE-22**, 1174 (1986).
[15] S. Wieczorek and W.W. Chow, Phys. Rev. A **69**, 033811 (2004).
[16] E. Doedel *et al.*, http://sourceforge.net/projects/auto2000/.
[17] C. Grebogi, E. Ott, and J. A. Yorke, Phys. Rev. Lett. **48**, 1507 (1982).